Available online at www.sciencedirect.com

ScienceDirect

Procedia Engineering 139 (2016) 76 – 86

Procedia Engineering

www.elsevier.com/locate/procedia

MRS Singapore – ICMAT Symposia Proceedings

8th International Conference on Materials for Advanced Technologies

Low Stress Encapsulants? Influence of Encapsulation Materials on Stress and Fracture of Thin Silicon Solar Cells as Revealed by Synchrotron X-ray Submicron Diffraction

Karthic Narayanan RENGARAJAN[1], Ihor RADCHENKO[1], Gregoria ILLYA[2], Vincent HANDARA[2], Martin KUNZ[3], Nobumichi TAMURA[3], Arief Suriadi BUDIMAN[1#]

[1]SUTD Singapore University of Technology and Design, Singapore, [2]Center for Solar Photovoltaics (CPV), Surya University, Indonesia,
[3]Advanced Light Source (BL 12.3.2), LBNL, Berkeley, CA, USA,
[#]Corresponding author, asbudiman@sutd.edu.sg,

Abstract

We study the effect of two polymer encapsulations with different material properties such as Young's modulus (E), yield strength etc. on the residual stress of mono-crystalline silicon. We observe through synchrotron X-ray microdiffraction that, solar photovoltaic (PV) module laminated with encapsulants A (soft) and B (stiff) which have Young's modulus of 6.34 and 28.32 MPa respectively, reveals distinct variations in residual stress of silicon. The stress of silicon measured near the solder (stress concentration region), showed a maximum quantitative value of ~ 300 MPa with encapsulant A whereas for the solar PV with encapsulant B, it showed a much higher value of ~ 450 MPa. Further correlation of stress to fracture/crack initiation events of silicon were also understood using three point bending tests. The result shows that with encapsulant A, crack initiation of silicon at a mean force of ~ 1.2 KN is observed whereas for the PV with encapsulant B, silicon cracked at much lower force of ~ 0.3 KN. These studies confirm that encapsulant materials have a significant effect on the residual stress of silicon, which directly affects the working efficiency and reliability of the solar PV.

Selection and/or peer-review under responsibility of the scientific committee of Symposium 2015 ICMAT

Keywords: Solar Cell; Silicon Stress; Synchrotron X-ray Micro-Diffraction; Silicon Cell Fracture;

Selection and/or peer-review under responsibility of the scientific committee of Symposium 2015 ICMAT
doi:10.1016/j.proeng.2015.09.230

1. Introduction

Recently, there has been strong commercial push in silicon-based solar PV industries especially towards enabling thinner and thinner silicon solar cells (< 150 μm) due to the significant cost reduction associated with it. Even though the module becomes thinner, the solar PV needs to have a lifetime operation of more than 20 years, to be considered as a cost effective solution [1, 2]. In the field, the PV module is always under the influence of various external loading conditions such as mechanical loads due to wind, snow, etc. and environmental conditions i.e. extreme temperature, thermal cycles, etc. These external factors increase the built-in stress, in addition to the inherent residual stresses developed during the processing such as lamination etc. Further, this eventually leads to fracture events thereby affecting the efficiency and reliability of the solar PV module [3–5]. Currently, in the solar PV community, there is large interest and focus on understanding the role of lamination materials and processes, in addition to the soldering materials and processes [6]. The encapsulant material used in solar PV industry must satisfy several different requirements, which include high optical trans- mittance of incident light, good dielectric properties (electrically insulating), mechanical compliance to protect the solar cells from external mechanical loads and stresses induced by differences in thermal expansion coefficients, good adhesion to both glass and silicon solar cells [3]. Silicones as an alternative encapsulation material were experimented by Ketola et al. [7]. Their objective of using this material was based on high transparency offered in the UV-visible wavelengths, wide range of refractive indices and excellent tolerance to high optical flux. Hurter et al. [8] also assessed glass fiber reinforced plastics (GFRP) composite materials as en- capsulation to study the electrical and thermal efficiency of the solar PV. Studies pertinent to solely effect of encapsulation material properties and its relation to building up of the PV residual stress are rather limited and have not been much reported in the literature. Recently, Dietrich et al. [6] have experimentally characterized the in-plane fracture strength of the solar PV module comparing two different encapsulation materials namely EVA having high and low stiffness properties. Their results clearly show that, PV module encapsulated with high stiffness EVA cracked at lower load whereas module resisted high load before initiation of crack, when encapsulated with the low stiffness EVA. Similarly Mickiewicz et al. [9] also analysed the encapsulation material stiffness at cold environmental conditions and subsequently its effect on the fracture of the solar PV module.

This preliminary evidence on the effect of laminating materials and pro- cesses motivated us to understand the basic mechanisms, thus opening the re- search gap for fundamental and quantitative investigation of the stress which is the driving force of fracture, therefore the subject of this paper. Studying how the effect of the encapsulant on the stress level after the lamination pro- cess will be crucial in highlighting the propensity to fracture in the thin silicon solar cells. Since it is the effect of the lamination material, we study the stress gradients of silicon cell while it is already encapsulated/laminated and thus the synchrotron X-ray microdiffraction is the unique technique, which allows us to map this evolution of stress [10]. The silicon wafer here was already encapsulated by ~ 0.5 mm of transparent polymers on each side. But with the high penetration of hard X-ray synchrotron radiation, we still could get the reflection from the silicon even though it was buried under 0.5 mm of encapsulant polymer material. This is a unique capability as it allows stress and microstructure evolution examination of silicon solar cells for instance during high temperature lamination process, or even during the operation (in operando) of the laminate, such as during thermal cycle or mechanical loading operation. Also, this kind of study is not hitherto possible using charged particle microscopy technique such as SEM and TEM or surface sensitive techniques such as micro-Raman spectroscopy. This technique could further lead to unravelling of potentially important and critical insights about what is really happening in the solar cell during lamination or what the deformation mechanisms are in the silicon solar cells during thermal cycling or mechanical loading. Our recent study on solar cells has garnered attention at the Advanced Light Source (ALS), Berkeley Lab Science Highlight [11].

In this study we use two different encapsulation materials namely an industry standard EVA (encapsulant A) and a commercially available thermoplastic (encapsulant B). Both the materials are then used as a lamination for the solar PV module. Then, solar PV module laminated with materials A and B are characterized for residual stress using synchrotron X-ray microdiffraction at Advanced Light Source (ALS) beamline 12.3.2. We further conducted three point bending tests of the PV module to understand the fracture/crack initiation mechanisms.

2. Experimental

A series of PV mini modules/laminates (one-cell coupons with commercially available monocrystalline silicon solar cells inside) were prepared using the two different encapsulants: an industry standard EVA (encapsulant A) and a commercially available thermoplastic (encapsulant B). Every laminated mini module consists of a glass, a front encapsulant layer, a 125 mm x 125 mm monocrystalline silicon solar cell, a back encapsulant layer and finally a backsheet. Stress measurements in the silicon around the solder joint were performed by synchrotron X-ray micro-diffraction (beamline 12.3.2) at the Advanced Light Source (ALS) of the Lawrence Berkeley National Labora- tory. Three point bending tests of the PV module were also conducted to investigate the fracture.

2.1 Synchrotron X-ray Microdiffraction

The X-ray characterization was performed at the Advanced Light Source (ALS) of the Lawrence Berkeley National Laboratory, beamline 12.3.2 [12, 13]. The polychromatic X-Ray beam produced from a superconducting mag- net source is refocused at the entrance of the experimental hutch by a 700 mm-long platinum-coated silicon toroidal mirror operating at a grazing an- gle of 4.5 mrad. Final focusing is done by Kirkpatrick-Baez (KB) focusing mirrors consisting of an orthogonal pair of 100 mm long tungsten coated silicon substrate bent to an elliptical shape. The Synchrotron X-ray micro- diffraction has nominally 0.8 μm × 0.8 μm focused beam size. The sample (Figure 1) sits on a XY high precision stage (range of 10 cm), which is mounted on a coarse XYZ Huber stage (range of ±15 mm in X, Y and Z). The diffraction patterns are collected with a DECTRIS Pilatus 1 M pixel area detector (active area of 179 × 169 mm2) which is placed at a distance of approximately 140 mm from the sample. The CCD detector is comprised of pixels, from which the relative change in position and size of the peak is extracted. The resolution of this CCD detector used in the current study is ∼ 0.03◦ [13]. The experimental setup in the beamline 12.3.2 provides the capabilities to obtain both kind of stress components i.e. deviatoric and hy- drostatic [14–16]. The technique at ALS beamline 12.3.2 has previously been found effective to map silicon cell stress, investigate plasticity of crystalline materials at submicron and nanometer scales etc. [17–28]

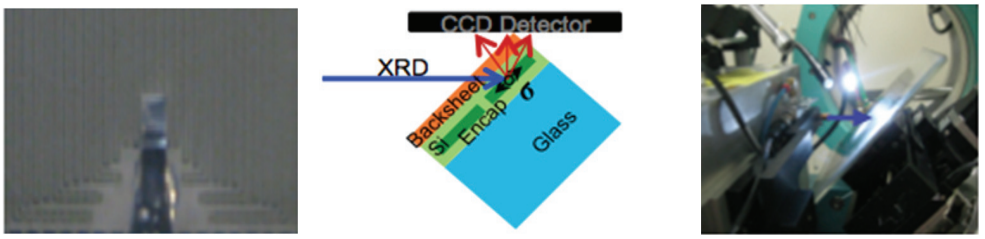

Fig. 1: a. Image of silicon cell around solder joint, b. The incoming synchrotron focused X-ray beam (the blue arrow) penetrates through the transparent backsheet layer (orange colored) and the back-side encapsulant layer (light green colored) and is diffracted by the silicon crystal (red arrows) allowing its crystallographic information to be captured by the CCD (Charge-Coupled Device) detector (black colored), which can then be translated into stress and, thus, crack propensity information and c. The in situ experimental using synchrotron X-ray micro diffraction, where the encapsulated mini module sits on a XY piezoelectric sample stage tilted at 45◦.

2.2 Mechanical Characterization

2.2.1 Tensile Tests

The tensile mechanical properties of encapsulants A and B at room temperature (∼ 25◦C) were measured using the Instron testing machine. The initial samples were 25 mm wide (W) with a total length of 150 (L) mm,

which was kept constant for all the tests. An initial thickness of 0.42 (sample A) and 0.46 mm (sample B) respectively were noted. For testing, aluminium tabs were bonded to the soft samples using an adhesive, which helped in preventing the erosion during gripping. An extensometer with a gauge length (lo) of 50 mm was used to measure the engineering strain (e = △l/lo), as shown in the Figure 2a. Different displacement rates of 10, 100 and 200 mm/min were applied and the corresponding load - displacement were recorded for ten samples at each of this testing condition. The samples were strained to a value of 0.3 (mm/mm), which was close to the maximum limit of the extensometer displacement (25 mm) and thereby, the tests were stopped. The samples after the end of the tests are shown in Figure 2b.

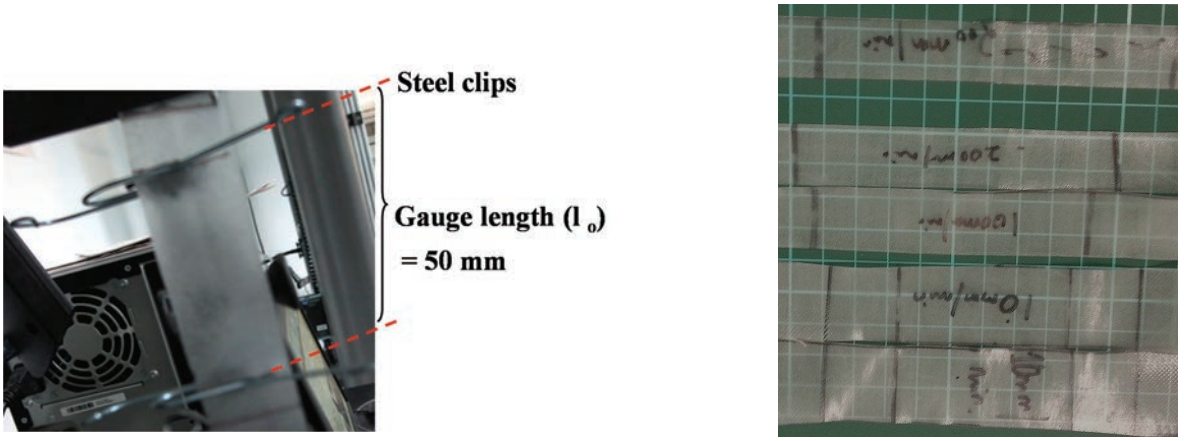

(a) Extensometer (steel clips) mounted at the gauge length. (b) Samples at the end of the test.

Fig. 2: Tensile testing of Encapsulation Materials

2.2.2 Dynamic Mechanical Analysis

Dynamic mechanical analysis (DMA) was also used to test the high temperature viscoelastic properties of the encapsulation materials A and B. An equal sample length of 20 mm was used for this testing. Since the samples being soft and compliant, the tests were run using the tension mode set up. All the samples (five from each material) were subjected to a temperature range of $\sim 20 - 100^{\circ}C$ with a heating rate of $4^{\circ}C$/min. The test condition was kept constant for all the samples.

2.3 In-Laminate Three point bending Tests

An in-laminate three point bending set up as shown in Figure 3 was used to conduct the tests. In this test, a PV coupon is placed on two parallel supporting pins with a distance of 10 cm. A uniform quasi static loading is monotonically applied in the centre of the glass by means of a loading pin (the maximum force of the load cell 50 ± 5% KN). The supporting and loading pins are mounted in a way, allowing the samples to freely rotate about axis parallel to the pin axis.. As the load is increased monotonically, visual inspection was conducted via a camera, which transmits the magnified images to a computer to allow visual/manual detection of macro scale cracks in the silicon solar cells. At the first sight of macro scale cracks in the silicon solar cells, the loading force was noted and later indicated as “Characteristic Strength” of the encapsulated solar cells in Section 3.3.

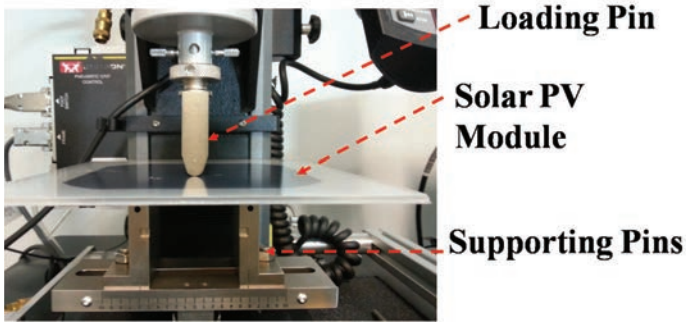

Fig. 3: Three Point Bending Test Set-up

3. Results

The results of quantitative residual stress of the silicon measured in the laminated PV module using the synchrotron X-ray source is presented followed by the mechanical properties of the two encapsulation materials A and B. Further, to experimentally simulate the environmental loading such as snow, wind etc., investigations were carried out using three point bending test to characterize the fracture initiation of the solar PV module.

3.1 Residual Stress Map of Silicon Cell

The stresses on the silicon near the solder joint (stress concentration region) were determined from the out-of-plane orientation of the Si (100) planes at any given pixel of the raster scanning using XMAS code [14]. 3D crystal orientations of silicon were obtained from indexing the silicon Laue pattern. A methodology called “adaptive indexing” allows tracking the silicon reflections below the metallization layers thus enabling us to obtain the silicon 3D orientation information even after encapsulation. Curvature from all 3 directions (X, Y and Z) can thus be obtained. As we can see in Figures 4a and 4b, the X-ray beam could not penetrate through the very thick solder joint and bus-bar and thus the dark region in the stress map indicating no information about silicon crystallography/stress was obtained from those pixels. Apart from that, the X-ray beam was able to probe through the metallization layer and other materials, and thus we could obtain the silicon crystal stress everywhere else. The effect of the metallization lines could still be seen on the left and right of the lower part of the scanning. This is also expected as metallization lines are the regions where the stresses are expected to be higher due to mismatch of coefficient of thermal expansion (CTE) between silicon and the metal (i.e. Cu in this case).

Our objective here is to measure the stress of the silicon as the effect of each encapsulant material. The stress map of the silicon with encapsulant A is shown in Figure 4a. It can be seen that the in-plane stress state (along X) of the silicon solar cell is in tensile (Red to green color, amounting about minimum 200 MPa). The nature of stress (tensile) in the silicon cell (in-plane, along X) agrees well with the stress-strain distribution map obtained through modeling as reported by S.Dietrich et al. [6]. The highest stresses seemed to be right around the solder joint (the red colored regions) amounting to about ~ 300 MPa. Figure 4b shows the stress mapping of the silicon with encapsulant B. Observations of stress state near the solder joint is similar with higher tensile than the one with encapsulant A. The highest stress was also found to be right around the solder joint (the red colored regions) amounting to about ~ 450 MPa. From these results, it shows that encapsulation material property has substantial effect on the residual stress of silicon. We further analyze the encapsulation material properties and its correlation to fracture, which will be discussed in the following sections.

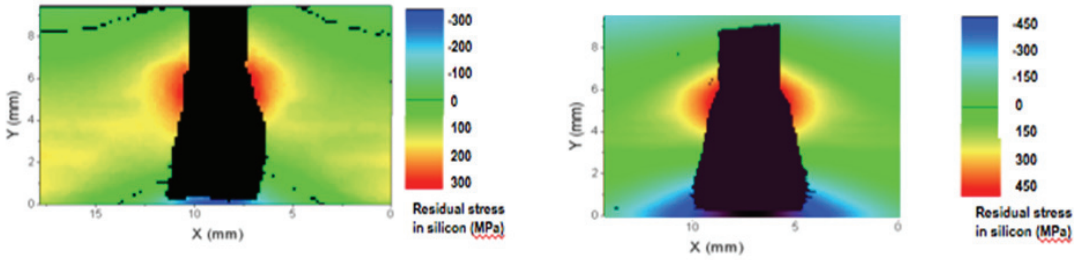

(a) (b)

Fig. 4: Residual stress map of silicon cell near the solder joint of solar PV module, laminated with a. Material A, and b. Material B.

3.2 Encapsulation Polymer Material Properties

The representative engineering and true stress vs. strain of samples A and B tested at a displacement rate of 100 mm/min is shown in Figure 5a. The engineering strain directly measured from extensometer is converted to true strain $\varepsilon_T = ln\,(1 + e)$. Similarly the engineering stress σ_e calculated based on the original cross sectional area (A_o) of the samples is used to obtain the true stress, $\sigma_T = \sigma_e*(1+e)$. The Young's modulus E obtained from the slope of the linear true stress region is shown in Figure 5b with respect to various displacement rates. From the results of Young's modulus i.e. stiffness vs. displacement rate, it can be seen that, sample A tested at displacement rate of 10 mm/min has lower mean modulus of 6.34 MPa compared to sample B which shows much higher value of 28.32 MPa, tested at the same condition. Moreover, the modulus values measured at different strain rates such as 100 and 200 mm/min also show similar behavior. The Young's modulus of sample A is 10.79 and 11.81 MPa respectively whereas sample B shows a value of 32.41 and 36.51 MPa for the same displacement rates of 100 and 200 mm/min. Further comparing the Young's modulus of samples A and B, it can be clearly observed that sample B is approximately three to four times stiffer as compared to sample A for all the displacement rate conditions.

From the DMA results, the storage modulus obtained from the high temperature tensile testing of both the encapsulation materials A and B are also shown in Figure 5c. The results show that, sample B has almost two orders (log scale) higher storage modulus compared to sample A at all temperatures from $\sim 20 - 100^{\circ}$C. This also confirms our previous observations that, the sample B is stiffer than A and does not show signs of significant softening even at high temperature (100^0 C).

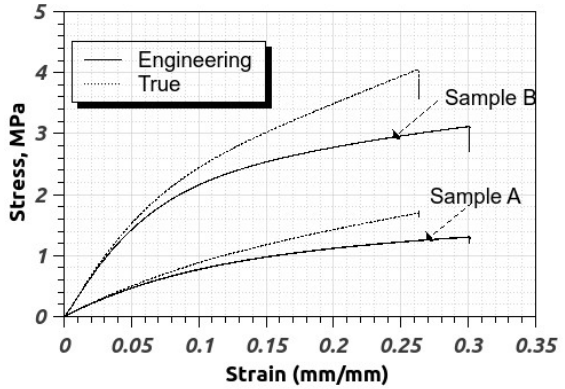

(a) Representative stress vs. strain curves at displacement rate of 100 mm/min

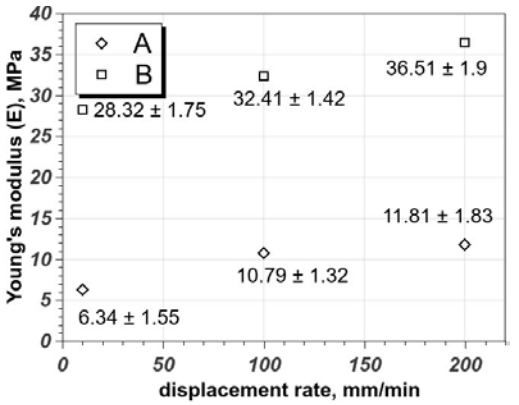

(b) Young's modulus at various displacement rates.

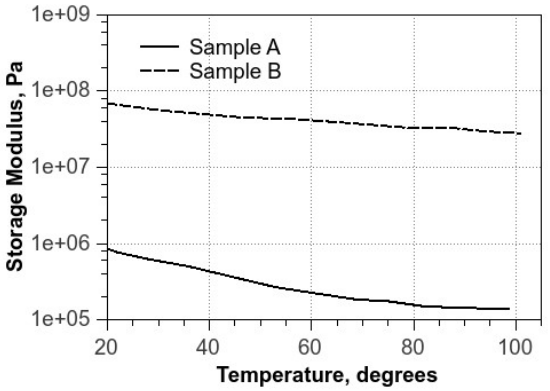

(c) Representative DMA (tension mode) curve of storage modulus vs. temperature

Fig. 5: Mechanical Properties of the encapsulation materials A and B

3.3 Fracture Observations

The characteristic fracture load of the solar PV obtained from the three point bending tests of the samples from both group (20 from each) is shown in Figure 6. The samples were subjected to multiple load steps of 30 N each and monitored for crack initiation through visual inspection. Visual inspection is not the ideal way here to detect cracks in the solar cells – an electro-luminescence (EL) should really be used. However, due to lack of facilities in our new university (SUTD), this method of crack detection/inspection was used to obtain a rough estimate of the fracture load. A load drop during the test was also a key parameter to check the crack initiation. When obvious crack propagation was found, the tests were stopped at those loads and the readings were noted. The results show a mean fracture load of ~ 1.2 KN for PV laminated with encapsulation material A, whereas for specimens encapsulated with material B, the mean fracture load dropped considerably to ~ 0.3 KN. These

observations show that, PV with encapsulant A can resist higher external loads i.e. both mechanical and environmental before failure.

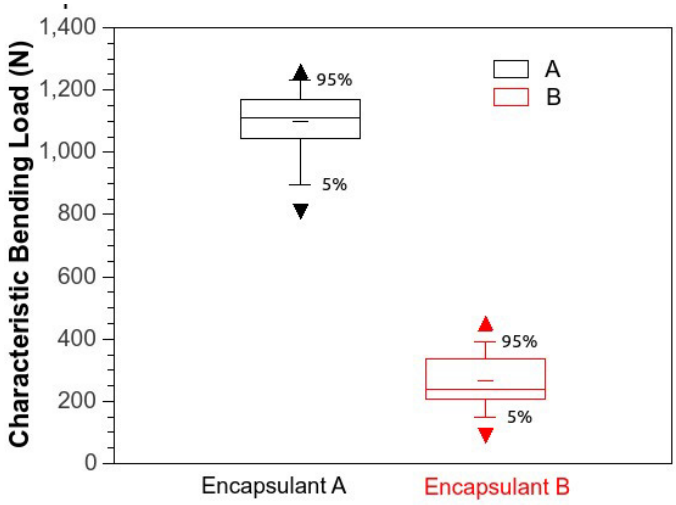

Fig. 6: Fracture results of solar PV encapsulated with materials A and B

It is worth mentioning here that the silicon solar cells are back-contacted and the solder joints are on the bottom side in Figure 3, although due to the thickness of the glass in this assembly (i.e. 3 mm), the whole thickness of the silicon solar cells here is under tensile stress. Cracks do tend to initiate in the bottom side of the silicon solar cells (due to slightly higher tensile stress), but they also tend to transmit through the thickness of the silicon due to single-crystalline nature of the samples used here thus appearing on the upper side almost the same time they were initiated on the bottom side, given the increasing bending load. The fact that the upper side of the solar cells are black colored also provides better contrast for the crack detection. Furthermore, these results do suggest significant difference in the signals from the two groups (beyond statistical requirements). This gave us more confidence in the data. In addition, similar studies by other groups [3, 9] have also concluded that different encapsulation materials could lead to distinct fracture propensity of the PV mini modules with otherwise the same, nominal silicon solar cells inside.

4. Discussion

Mechanical stress and fracture The laminated PV mini-modules, encapsulated with this two materials A and B show distinct variations of residual stress in silicon near the solder region as revealed by Synchrotron X-ray microdiffraction (Figures 4aand 4b) which is expected based on the different material stiffness property. From the mechanical properties of the encapsulation materials used in this study: an industry standard EVA (encapsulant A) and a commercially available thermoplastic (encapsulant B), it is distinctively clear from Figure 5b that, material B is approximately three to four times stiffer than A. Viscoelastic behavior (Figure 5c) to understand these materials at near lamination processing temperature (150◦C), shows similar observations. The encapsulation material B is stiffer even at the maximum test temperature of 100◦C as compared to encapsulant A. During lamination (at high temperature of 150◦C), the lamination pressure might give rise to additional stress con- centration when the solar cells with very inhomogeneous topology (due to solder joints and metallization bars, etc.) were pressed against a stiffer encapsulant (compared to a softer one). This could lead to much higher stress concentration (~ 450 MPa) in the silicon solar cells of Samples B (with stiffer encapsulant), thus leading to much earlier crack initiation and

propagation (at 0.3 KN of bending force). While for Samples A, due to its softer encapsulant, the pressure from the laminator might give rise to lower stress concentration (~ 300 MPa) in the silicon solar cells and thus leading to much delayed crack initiation and propagation (at 1.2 KN of bending force). This could be one of the possible explanations, however the exact mechanisms leading to the phenomenon observed in this study are a subject of our continued investigations.

The effect of the solder joint on the stress concentration on silicon solar cells is obviously noted, but as both groups of samples used nominally the same silicon solar cells (from the same production batch, etc.) with the same solder joints materials and processes (save for a minimum high-volume manufacturing variation), the effect of the solder joint on the stress concentration on silicon solar cells in both groups of Samples, A and B, would be nominally the same. Thus the difference observed in terms of residual stress on silicon solar cells as well as the load at which fracture events start occurring could be solely attributed to the difference in the encapsulants. Further analysing the fracture, residual stress indeed mimics like a pre-notch which under a homogeneous loading, aids in the crack initiation and propagation. The in-plane stresses of the mono-crystalline silicon were all tensile (Figures 4a and 4b) and the highest compared to other components of the PV module [6]. Based on the bending theory, during the loading, the maximum in-plane tensile stresses accumulated during lamination will obviously increase from the solder (supporting pin side) and we suspect that, crack would have initiated from there. This is supported based on results of Schroder et al. [5], who also showed that the silicon cracks from the bottom side during the bending tests.

5. Conclusions

This study has investigated the effect of lamination material property on the residual stress of mono-crystalline silicon solar cell using Synchrotron X-ray microdiffraction, Advanced Light source (beamline 12.3.2). The following conclusions from this study are:

- Solar PV laminated with encapsulation materials A (Soft) and B (Stiff) shows different residual stress of silicon cell (Figures 4a and 4b). The residual stress of silicon with material A shows a maximum value of ~ 300 MPa near the solder whereas with material B shows ~ 450 MPa.
- The characteristic fracture load of the PV encapsulated with material A shows ~ 1.2 KN compared to ~ 0.3 KN for PV laminated with material B.
- The exact mechanisms leading to these findings are a subject of our continued investigations, which could lead to a low stress encapsulation technology that would potentially have a great impact to the viability of the solar PV technology to replace the fossil-based energy sources.

Acknowledgements

The authors gratefully acknowledge the samples and support provided by Dr. Alexander Caldwell of SUNPOWER for the synchrotron X-ray experiments. Critical support and infrastructure provided by Singapore University of Technology and Design (SUTD) during the manuscript preparation is much appreciated. ASB and KRN also gratefully acknowledge the funding and support from National Research Foundation (NRF)/Econcomic Development Board (EDB) of Singapore for the project under EIRP Grant *"(NRF2013EWT- EIRP002-017) - Enabling Thin Silicon Technologies for Next Generation, Lower Cost Solar PV Systems*". The Advanced Light Source (ALS) (supported by the Director, Office of Science, Office of Basic Energy Sciences, and Materials Sciences Division, of the U.S.Department of Energy under Contract No. DE-AC02-05CH11231 at Lawrence Berkeley National Laboratory and University of California, Berkeley, California). The move of the micro-diffraction program from ALS beamline 7.3.3 onto to the ALS superbend source 12.3.2 was enabled through the NSF grant #0416243.

References

[1] A. Gabor, M. Ralli, L. Montminy, S. Alegria, C. Bordonaro, J. Woods, and J. Felton. Soldering induced damage to thin Si solar cells and detection of cracked cells in modules. 21st European Photovoltaic Solar Energy Conference, 2006.

[2] M. Sander, S. Dietrich, M. Pander, M. Ebert, and J. Bagdahn. System- atic investigation of cracks in encapsulated solar cells after mechanical loading. Solar Energy Materials & Solar Cel ls, 111:82–89, 2013.

[3] M. Sander, S. Dietrich, M. Pander, S. Schweizer, M. Ebert, and J. Bag- dahn. Investigations on crack development and crack growth in em- bedded solar cells. Proceedings of SPIE –The International Society for Optical Engineering, 2011.

[4] M. Kontges, I. Kunze, S. Kajari-Schroder, X. Breitenmoser, and B. BjÃžrneklett. The risk of power loss in crystalline silicon based pho- tovoltaic modules due to micro-cracks. Solar Energy Materials and Solar Cel ls, 95:1131–1137, 2011.

[5] S. Kajari-Schroder, I. Kunze, U. Eitner, and M. Kontges. Spatial and orientational distribution of cracks in crystalline photovoltaic modules generated by mechanical load tests. Solar Energy Materials and Solar Cel ls, 95:3054–3059, 2011.

[6] S. Dietrich, M. Pander, M. Sander, S.H. Schulze, and M. Ebert. Mechan- ical and Thermo-Mechanical Assessment of Encapsulated Solar Cells by Finite-Element-Simulation. Proceedings of SPIE –The International So- ciety for Optical Engineering, 2008.

[7] B. Ketola, K. R. McIntosh, A. Norris, and M. K. Tomalia. Silicones For Photovoltaic Encapsulation. 23rd European Photovoltaic Solar Energy Conference, 2008.

[8] W. Hurter, G. Oosthuizen, and N. Janse van Rensburg. Investigating the Effects of Composite Materials in Solar Cell Encapsulation. Inter- national Conference on Competitive Manufacturing, 2013.

[9] R. Mickiewicz, B. Li, D. Doble, T. Christian, J. Lloyd, A. Stokes, C. Voelker, Winter. M, B. Ketola, A. Norris, and N. Shephard. Effect of Encapsulation Modulus on the Response of PV Modules to Mechanical Stress. 26th European Photovoltaic Solar Energy Conference, 2011.

[10] A.S. Budiman, G. Illya, V. Handara, A. Caldwell, C. Bonelli, M. Kunz, N. Tamura, and D. Verstraeten. Enabling Thin Silicon Technologies for Next Generation c-Si Solar PV Renewable Energy Systems using Syn- chrotron X-ray Microdiffraction as Stress and Crack Mechanism Probe. Solar Energy Materials and Solar Cel ls, 130:303–308, 2014.

[11] A.S. Budiman. Enabling Thin Silicon Solar Cell Technology, http://www-als.lbl.gov/index.php/science-highlights/industry-als/829- improving-thin-silicon-solar-cell-technology.html, June 2013.

[12] A. A. MacDowell, R. S. Celestre, N. Tamura, R. Spolenak, B. Valek, W. L. Brown, J. C. Bravman, H. A. Padmore, B. W. Batterman, and J. R. Patel. Submicron X-ray diffraction. Nuclear Instruments & Meth- ods In Physics Research Section A-accelerators Spectrometers Detectors and Associated Equipment, 467:Berliner Elektronenspeicherring Gesell Synchrotronstrahlung (BESSY), 2001.

[13] N. Tamura, R. S. Celestre, A. A. MacDowell, H. A. Padmore, R. Spole- nak, B. C. Valek, N. M. Chang, A. Manceau, and J. R. Patel. Submicron X-ray diffraction and its applications to problems in materials and en- vironmental science. Review of Scientific Instruments, 73:1369–1372, 2002.

[14] N. Tamura, A. A. MacDowell, R. Spolenak, B. C. Valek, J. C. Bravman, W. L. Brown, R. S. Celestre, H. A. Padmore, B. W. Batterman, and J. R. Patel. Scanning X-ray microdiffraction with submicrometer white beam for strain/stress and orientation mapping in thin films. Journal of Synchrotron Radiation, 10:137–143, 2003.

[15] N. Tamura, H. A. Padmore, and J. R. Patel. High spatial resolution stress measurements using synchrotron based scanning X-ray microd- iffraction with white or monochromatic beam. Materials Science and Engineering A-structural Materials Properties Microstructure and Pro- cessing, 399:92–98, 2005.

[16] N. Tamura, M. Kunz, K. Chen, R. S. Celestre, A. A. MacDowell, and T. Warwick. A superbend X-ray microdiffraction beamline at the ad- vanced light source. Materials Science and Engineering A-structural Materials Properties Microstructure and Processing, 524:28–32, 2009.

[17] A. S. Budiman, W. D. Nix, N. Tamura, B. C. Valek, K. Gadre, J. Maiz, R. Spolenak, and J. R. Patel. Crystal plasticity in Cu damascene in- terconnect lines undergoing electromigration as revealed by synchrotron X-ray microdiffraction. Applied Physics Letters, 88:233515 (1–3), 2006.

[18] A. S. Budiman, S. M. Han, J. R. Greer, N. Tamura, J. R. Patel, and W. D. Nix. A search for evidence of strain gradient hardening in Au submicron pillars under uniaxial compression using synchrotron X-ray micro diffraction. Acta Materialia, 56:602–608, 2008.

[19] G. Feng, A. S. Budiman, W. D. Nix, N. Tamura, and J. R. Patel. In- dentation size effects in single crystal copper as revealed by synchrotron X-ray microdiffraction. Journal of Applied Physics, 104:043501, 2008.

[20] K. Chen, N. Tamura, B. C. Valek, and K. N. Tu. Plastic deformation in Al (Cu) interconnects stressed by electromigration and studied by synchrotron polychromatic x-ray microdiffraction. Journal of Applied Physics, 104(1):013513, 2008.

[21] A. S. Budiman, P. R. Besser, C. S. Hau-Riege, A. Marathe, Y. . C. Joo, N. Tamura, J. R. Patel, and W. D. Nix. Electromigration-Induced Plas- ticity: Texture Correlation and Implications for Reliability Assessment. Journal of Electronic Materials, 38:379–391, 2009.

[22] A. S. Budiman, C. S. Hau-Riege, W. C. Baek, C. Lor, A. Huang, H. S. Kim, G. Neubauer, J. Pak, P. R. Besser, and W. D. Nix. Electromigration-Induced Plastic Deformation in Cu Interconnects: Effects on Current Density Exponent, n, and Implications for EM Relia- bility Assessment. Journal of Electronic Materials, 39:2483–2488, 2010.

[23] A. S. Budiman, N. Li, Q. Wei, J. K. Baldwin, J. Xiong, H. Luo, D. Trug- man, Q. X. Jia, N. Tamura, M. Kunz, K. Chen, and A. Misra. Growth and structural characterization of epitaxial Cu/Nb multilayers. Thin Solid Films, 519:4137–4143, 2011.

[24] A. S. Budiman, S.M. Han, N. Li, Q.M. Wei, P. Dickerson, N Tamura, M Kunz, and A Misra. Plasticity in the nanoscale Cu/Nb single- crystal multilayers as revealed by synchrotron Laue x-ray microdiffrac- tion. Journal of Materials Research, 27:599–611, 2012.

[25] A. S. Budiman, H. . A. . S. Shin, B. . J. Kim, S. . H. Hwang, H. . Y. Son, M. . S. Suh, Q. . H. Chung, K. . Y. Byun, N. Tamura, M. Kunz, and Y. . C. Joo. Measurement of stresses in Cu and Si around through-silicon via by synchrotron X-ray microdiffraction for 3-dimensional integrated circuits. Microelectronics Reliability, 52:530–533, 2012.

[26] H.A.S. Shin, B.J. Kim, J.H. Kim, S.H. Hwang, A.S. Budiman, H.Y. Son, K.Y. Byun, N. Tamura, M. Kunz, D.I. Kim, and Y.C. Joo. Microstruc- ture evolution and defect formation in Cu through-silicon vias (TSVs) during thermal annealing. Journal of Electronic Materials, 41:712 – 719, 2012.

[27] A. S. Budiman, G. Lee, M.J Burek, D. Jang, S. Han, N. Tamura, M. Kunz, J. R. Greer, and T. Y. Tsui. Plasticity of Indium nanostructures as revealed by synchrotron X-ray microdiffraction. Materials Science and Engineering A, 538:89–97, 2012.

[28] A. S. Budiman, Karthic.R. Narayanan, N. Li, J. Wang, N. Tamura, M. Kunz, and A. Misra. Plasticity evolution in nanoscale Cu/Nb single- crystal multilayers as revealed by synchrotron X-ray microdiffraction. Materials Science and Engineering A, 635:6–12, 2015.